

Article

Preparation of Multiscale α Phase by Heat Treatments and Its Effect on Tensile Properties in Metastable β Titanium Alloy Sheet

Hanyu Jiang ¹, Zhaoxin Du ^{1,2,*}, Da Wang ¹, Tianhao Gong ^{1,*}, Xiaoming Cui ¹, Fei Liu ¹, Jun Cheng ³ and Wenzhen Chen ⁴

¹ School of Materials Science and Engineering, Inner Mongolia University of Technology, Hohhot 010051, China; jianghanyu2020@163.com (H.J.); wangda274357513@163.com (D.W.); xmcui@imut.edu.cn (X.C.); ngdliufei@163.com (F.L.)

² Inner Mongolia Key Laboratory of Light Metal Materials, Inner Mongolia University of Technology, Hohhot 010051, China

³ Northwest Institute for Non-Ferrous Metal Research, Shaanxi Key Laboratory of Biomedical Metal Materials, Xi'an 710016, China; chengjun_851118@126.com

⁴ School of Materials Science and Engineering, Harbin Institute of Technology, Weihai 264209, China; nclwens@hit.edu.cn

* Correspondence: duzhaoxin@imut.edu.cn (Z.D.); gth@imut.edu.cn (T.G.)

Abstract: This study presents a strategy for the preparation of multiscale α phase by high/low-temperature two-step aging in metastable β titanium alloy, Ti-15Mo-3Al-2.7Nb-0.2Si. The purpose of high-temperature aging is to obtain a number of micro-scale secondary α phases (α_S), besides precipitation-free zones (PFZs). After that, in the second stage of low-temperature aging, the nano-scale tertiary α phase (α_T) precipitates in the PFZs. The second-step aging temperature and the time at low temperature will have an important effect on α_T . On the one hand, with the extension of aging time, the morphology of α_T changes from dot-like to needle-like. Secondly, the increase of the second-step aging temperature will promote precipitation of α_T in PFZs. The strength increases gradually with the accelerated precipitation of α_T , and good plasticity is still maintained. The effect of multiscale α on fracture behavior was investigated by in situ tensile testing. Results show that cracks form a transgranular fracture along the slip line after solution treatment. After first-step aging, the crack easily passes through α_S and forms an intergranular fracture. After second-step aging, the formation of multiscale α phase has a stronger effect in hindering the crack growth, which leads to crack propagation mainly by transgranular fracture. Overall, this study demonstrates that the alloy can be heat-treated to achieve an excellent match between strength and ductility, which is expected to meet the application requirements of structural materials of the new generation of aircraft.

Keywords: TB8 titanium alloy; duplex aging; multiscale α phase; in situ tensile testing; fracture behavior



Citation: Jiang, H.; Du, Z.; Wang, D.; Gong, T.; Cui, X.; Liu, F.; Cheng, J.; Chen, W. Preparation of Multiscale α Phase by Heat Treatments and Its Effect on Tensile Properties in Metastable β Titanium Alloy Sheet. *Metals* **2021**, *11*, 1708. <https://doi.org/10.3390/met11111708>

Academic Editors: Maciej Motyka and Thomas Niendorf

Received: 30 September 2021

Accepted: 22 October 2021

Published: 26 October 2021

Publisher's Note: MDPI stays neutral with regard to jurisdictional claims in published maps and institutional affiliations.



Copyright: © 2021 by the authors. Licensee MDPI, Basel, Switzerland. This article is an open access article distributed under the terms and conditions of the Creative Commons Attribution (CC BY) license (<https://creativecommons.org/licenses/by/4.0/>).

1. Introduction

Ti-15Mo-3Al-2.7Nb-0.2Si alloy is a metastable β -type titanium alloy. The alloy has the advantages of high strength, excellent cold and hot processing performance, strong oxidation resistance, and good corrosion resistance. It has a wide range of applications in the fields of airplane structure parts, engines, and aerospace [1].

The commonly used strengthening method of β titanium alloy is an aging treatment to precipitate high-density fine secondary α phase. The morphology, quantity, and distribution proportion of α phase can be controlled by different heat treatment processes, thereby achieving the purpose of improving the properties. It had been observed that the morphology and the volume fraction of α phase in aging treatments depend largely on treatment temperature, treatment time, heating/cooling rate, and grain size. Compared to

the single-step aging treatment, a duplex aging treatment appeared to increase the volume fraction of hexagonal close-packed (HCP) α phases, precipitate α phases finely, distribute uniformly, and reduce precipitation-free zones [2]. In the past few decades, many studies have focused on the effect of different aging processes on microstructure and properties of β titanium alloys [3–5]. Yumak et al. [6] showed that preaging treatment applied after cryogenic treatment prevented the formation of precipitation-free zones by providing a finer and more uniform distribution of α phases. Optimum mechanical properties were obtained in cryogenic treatment followed by 250 °C/10 h + 450 °C/20 h duplex aging treatment. Compared to the single-step aging treatment, the duplex aging treatment provided finer, higher-volume-fraction, and more uniform precipitation of the α phases in the alloy [7,8]. Generally speaking, the greater the density and the smaller the size of secondary α , the higher the strength that can be achieved in β alloy. Therefore, some researchers have proposed some methods (such as lowering the aging temperature, assisting nucleation by precursors, etc.) to reduce the size of secondary α phase to exploit the higher strength of β titanium alloy.

For example, Santhosh et al. [9] prepared α phase with fine size and high density through low/high temperature duplex aging, which made Ti-15V-3Cr-3Al-3Sn titanium alloy obtain high strength (1246 MPa) and high hardness (405 HV). The reason was that low-temperature aging provided a large number of uniformly distributed precursors for phase precipitation during the high-temperature aging process. As a result, the size of α precipitates is smaller and the volume fraction is higher. Furuhashi et al. [10] showed that fine α precipitates nucleate uniformly in the precursors of isothermal ω -particles during lower-temperature aging (300–400 °C). The uniform, fine, and dispersed secondary α phase can be obtained effectively by low/high temperature duplex aging, and the alloy shows an increase in strength. Mantri et al. [11,12] demonstrated that fine-scale α exhibited higher strengths compared to those containing coarser α precipitates by analyzing the crystal structure of fine α precipitates and an α/β interface composition profile using transmission electron microscopy (TEM) and atom probe techniques. They showed that the strength and elongation of the alloy can be controlled by tuning the scale of α precipitates via two-step aging. In addition, some scholars [13–15] adopted low-temperature aging to precipitate ω phase firstly, and then adopted high-temperature aging to precipitate α phase on the basis of ω phase. A fine and diffuse secondary α phase was finally obtained; therefore, the strength of β titanium alloy can be greatly improved. However, some research has shown that the fine dispersion of secondary α can not only improve the strength and hardness of β titanium alloy, but can also cause serious plastic loss. Chou et al. [16] found that the effective strengthening of the alloys by fine needle-like α precipitates impeded the dislocation motion and led to the limited ductility of these alloys, while the increase of strength was accompanied by a decrease of ductility. Previous studies by our team have stated that the refinement of secondary α phase can significantly improve the strength of titanium alloy, but the reduction of the size of secondary α phase will lead to a decrease in the plasticity of titanium alloy [17,18]. According to the research results of Yao et al. [19], the size of α phase increased but the number decreased with the increase of aging temperature, which improved the alloy plasticity: the plasticity increased from 4.7% to 7.9% due to the precipitation of coarse α phase.

As shown in the above analysis, fine and diffuse secondary α phases can obtain high strength and hardness, but plasticity is severely sacrificed, and coarse α phase can improve the ductility of the alloy. Therefore, this paper presents a strategy for preparation of multiscale α phase by high/low-temperature two-step aging. The purpose of a multiscale structure is to prepare any two kinds of microstructure or the microstructure of coexisting multi-scale grains on metal materials, including nanocrystalline (<100 nm), ultra-fine crystal (100–500 nm), microcrystalline (500 nm–2 μ m), coarse crystal (>10 μ m), and so on [20,21]. First, high-temperature aging was carried out to precipitate micron-sized (width) secondary α phase and retain some precipitate-free zones. Secondly, low-temperature aging is performed to precipitate nanoscale (width) tertiary α phase in the precipitate-free zones

(reserved in high-temperature aging). Finally, the α phases with different scales are formed to improve the comprehensive matching of strength and plasticity of β titanium alloy.

2. Materials and Methods

Ti-15Mo-3Al-2.7Nb-0.2Si titanium alloy material used in this experiment is a cold-rolled sheet with a thickness of 1 mm. The main chemical composition of the alloy is shown in Table 1. Chemical composition was determined by the manufacturer's certificate. The β transition temperature of the alloy measured by metallographic method is $815\text{ }^{\circ}\text{C} \pm 5\text{ }^{\circ}\text{C}$. The metallographic method was used for microstructure evaluation of the sample, which was quenched in the temperature range of $790\text{--}830\text{ }^{\circ}\text{C}$ with an interval of $10\text{ }^{\circ}\text{C}$, and a holding time of 1 h; the cooling method was water-cooling. The microstructural evolution was characterized by scanning electron microscopy (SEM) and transmission electron microscopy (TEM) techniques; both need to be used under vacuum conditions. Before SEM observation was carried out on Quanta FEG 650 (FEI Company, Hillsboro, OR, USA), the specimens were mechanically polished and etched in Kroll's reagent (10 mL HF, 30 mL HNO_3 , and 200 mL H_2O). TEM observation was performed on Philips-CM12 (FEI Company, Hillsboro, OR, USA). The TEM samples were prepared by grinding/polishing to $100\text{ }\mu\text{m}$ in thickness, followed by punching $3\text{ }\mu\text{m}$ diameter disks, and then prepared with twin-jet electrochemical polishing method. Then, the Philips APD-10 automatic diffraction analyzer (Oxford Instruments plc, Oxfordshire, UK) was used for X-ray diffraction (XRD) analysis. The test parameters were: Cu target, voltage of 15 V, scanning angle range of $20\text{--}80^{\circ}$, and scanning speed of $2^{\circ}/\text{min}$.

Table 1. Chemical constituents of Ti-15Mo-3Al-2.7Nb-0.2Si alloy (wt.%).

Element	Mo	Al	Nb	Si	O	Fe	H	N	C	Ti
Ti-15Mo-3Al-2.7Nb-0.2Si	14.9	3.06	2.74	0.21	0.005	0.02	0.0017	0.091	0.009	Bal.

The tensile specimen (Figure 1a) was prepared from the cold-rolled sheet by wire electrical discharge machining (WEDM). After being polished on sandpaper, the tensile specimen was subjected to Instron 5569 (Instron Company, Boston, MA, USA) universal testing machine for tensile test at a tensile speed of 1 mm/min. In order to ensure repeatability, each value is an average of three measurements. In situ tensile tests were performed under a field emission scanning electron microscope (SEM) Quanta FEG 650 (FEI Company, Hillsboro, OR, USA) with a tensile platform (dimensions shown in Figure 1b). Before the specimen was stretched, the samples used for microstructure observation were polished sequentially in water on 80, 400, 1000, and 2000 grid SiC abrasive paper, and then, electrochemical polishing was performed in a mixture of methanol, butanol, and perchlorate (6:3:1) in a solution environment at $-30\text{ }^{\circ}\text{C}$. Etching of SEM samples was performed in a solution of HF, HNO_3 , and H_2O (3:7:90). Tensile fracture surfaces were observed by SEM.

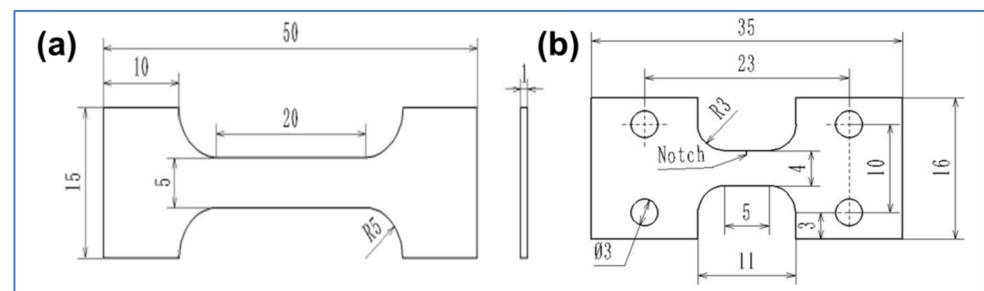


Figure 1. Dimension drawing of alloy (mm): (a) extension test, (b) in situ tensile test.

Samples were firstly solution-treated (solution treatment was defined as HT) for 0.5 h at $780\text{ }^{\circ}\text{C}$ (α/β region), followed by first-step aging (first-step aging was defined as SA) for 4 h at $650\text{ }^{\circ}\text{C}$. Finally, the samples were subjected to second-step aging (second-step aging

was defined as HLDA) for 5 min, 0.5 h, 2 h, and 4 h at temperatures ranging from 450 °C to 550 °C with an interval of 50 °C. All cooling methods were air-cooling. Coding designation and the parameters of heat treatment are given in Table 2.

Table 2. Coding designation and the parameters of heat treatment. HT: solution treatment. SA: first-step aging. HLDA: second-step aging.

Heat Treatment	Parameters of Heat Treatment		Coding Designation of Heat Treatment
	Temperature/°C	Time	
Solution treatment	780	0.5 h	HT
Plus first-step aging	650	4 h	SA
Plus second-step aging	450	5 min, 0.5 h, 2 h, 4 h	HLDA
	500		
	550		

3. Results and Discussion

3.1. Microstructure Observation

Figure 2a shows one microstructure of HT alloy. It can be seen that a small amount of equiaxed α phase distributed in the β matrix. The α phase precipitated in HT is referred to as primary α phase (α_p) here in order to distinguish the α phase precipitated during aging. Figure 2d shows the XRD patterns of HT and SA alloy. From the blue line, it can be seen that the content of α_p after HT is very small. The red line shows that the peak intensity of β phase decreased and the number of peaks of α phase increased after SA, which indicates that α phase precipitated during SA. Figure 2b,c present the microstructures after SA, showing that a certain amount of lath α precipitated from the matrix. The α phase precipitated in SA is referred to as secondary α phase (α_s) in order to distinguish the α phase precipitated during HLDA. In addition, due to the incomplete aging, there is a certain area of precipitate-free zones (PFZs) between micro-scale (width) α_s , as expected.

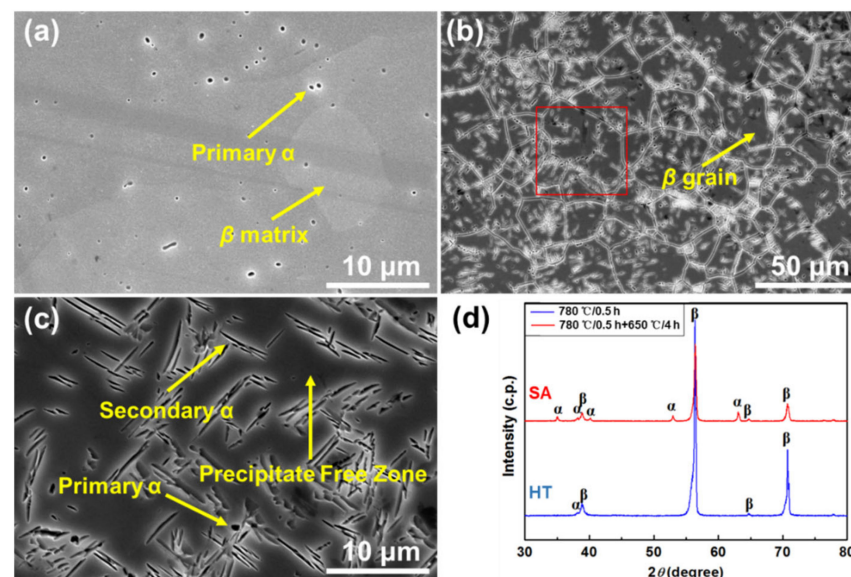


Figure 2. Microstructures of the alloy after heat treatment: (a) HT (solution treatment), (b,c) SA (first-step aging), (d) XRD (X-ray diffraction) patterns of HT (solution treatment) and SA (first-step aging).

Figure 3 shows a microstructure of HLDA alloy at the second-step aging temperature of 450 °C. Figure 3a–c show the microstructures after second-step aging for 5 min. The morphology of PFZs on the figure shows no significant change compared with SA (Figure 2c). However, there are some dot-like precipitates from PFZs when the second-step

aging time is extended to 0.5 h (Figure 3f). With aging time increases, the morphology of the precipitated phase from PFZs changes to needle-like (Figure 3i), and its quantity gradually increases (Figure 3l). Figure 4a shows the XRD patterns of HLDA alloy at the second-step aging temperature of 450 °C. It can be seen that the phase composition of HLDA is consistent with that of SA. Meanwhile, the peak intensity of α phase increases with the prolongation of the second-step aging time. This means that that more α phases precipitated, but no other phases were formed, even when aging at a lower temperature. In order to distinguish the precipitates of α phase during HLDA, it is denoted as tertiary α phase (α_T). The tertiary α phase is a nano-scale (width) phase.

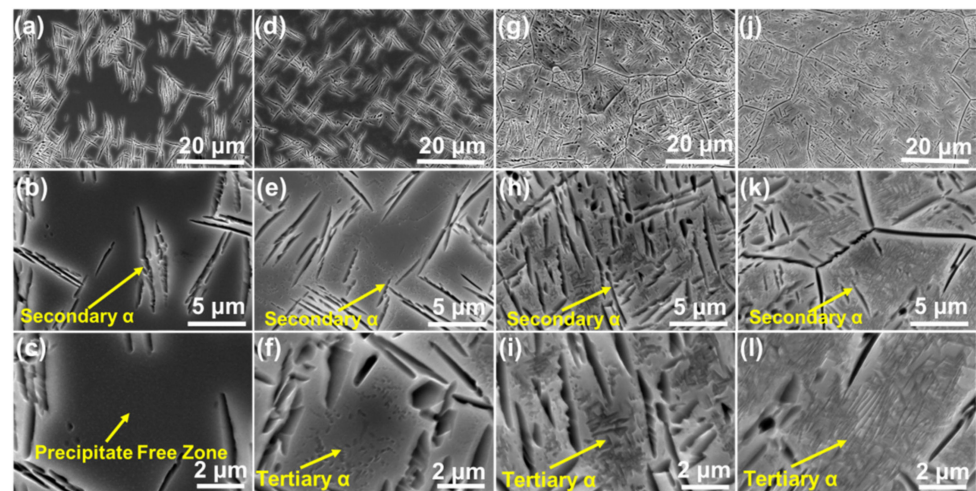


Figure 3. Microstructures of the alloy after HLDA (second-step aging) for different time at 450 °C: (a–c) 5 min, (d–f) 0.5 h, (g–i) 2 h, (j–l) 4 h.

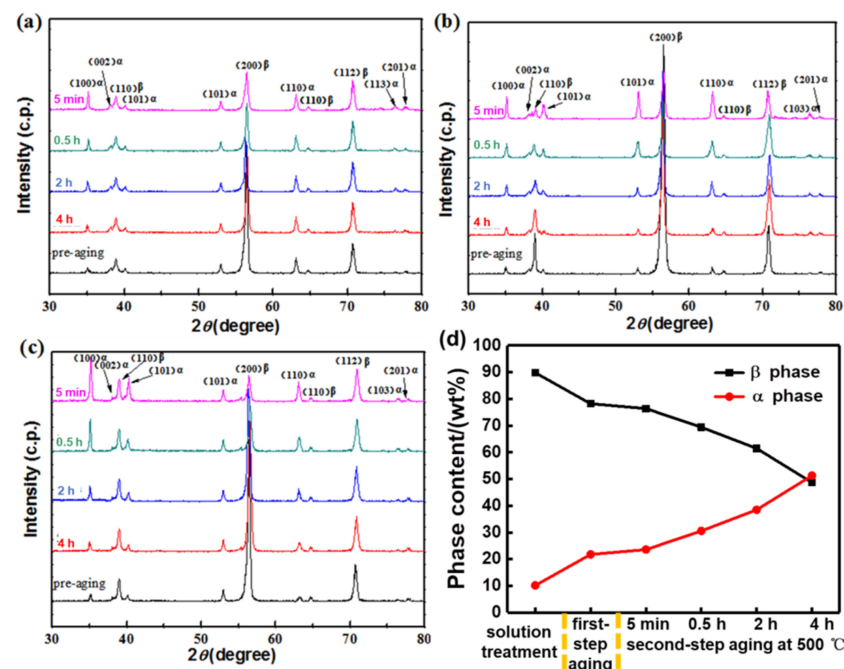


Figure 4. XRD pattern after HLDA at different temperature: (a) 450 °C, (b) 500 °C, (c) 550 °C, (d) phase content of 500 °C.

Figure 5 shows a microstructure of the HLDA alloy at the second-step aging temperature of 500 °C. Compared with HLDA at 450 °C, with the increase of aging time, the microstructure of HLDA alloy at 500 °C changed with the same trend at 450 °C, showing

the PFZs appeared as dot-like precipitation, and then transformed into needle-like α_T , the number of which increases continuously (Figure 5l). However, after HLDA at 500 °C, the size of the α_S slightly increases. The XRD pattern further shows that the general trend is that the content of α phase increased with the second-step aging time (Figure 4b). In addition, the phase content of XRD data obtained at 500 °C was calculated by phase K value (RIR) and diffraction intensity. The results showed that the content of α phase increased with aging time (Figure 4d).

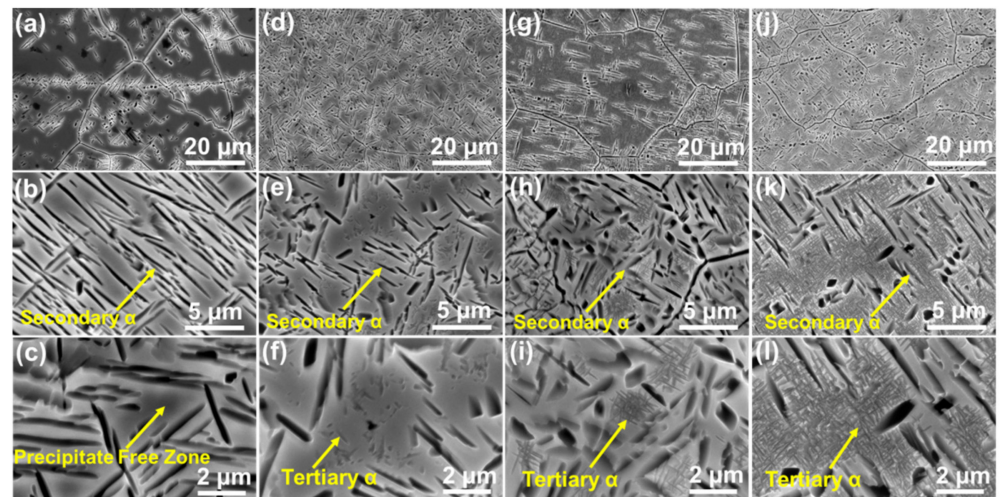


Figure 5. Microstructures of the alloy after HLDA for different time at 500 °C: (a–c) 5 min, (d–f) 0.5 h, (g–i) 2 h, (j–l) 4 h.

A microstructure of the HLDA alloy at the second-step aging temperature of 550 °C is shown in Figure 6. Different from 450 °C and 500 °C, the dot-like α_T has already been observed on the figure at 550 °C for 5 min, and it changed to a needle-like shape most obviously after 0.5 h, as shown in Figure 6a–f. According to Figures 3l, 4, 5l and 6l, increasing aging temperature can promote the precipitation of α_T , and the size of α_T is slightly increased. During the low-temperature aging process, sufficient time is needed to precipitate α phase. Even if the driving force for the nucleation is large, the driving force for growth is small. Therefore, at the same time, increasing the aging temperature provides more driving force for the precipitation of α phase [22]. The peak intensity of α phase is the highest after HLDA for 4 h at 550 °C (Figure 4c). At this time, the concentration of the α_T distribution of the alloy is the densest.

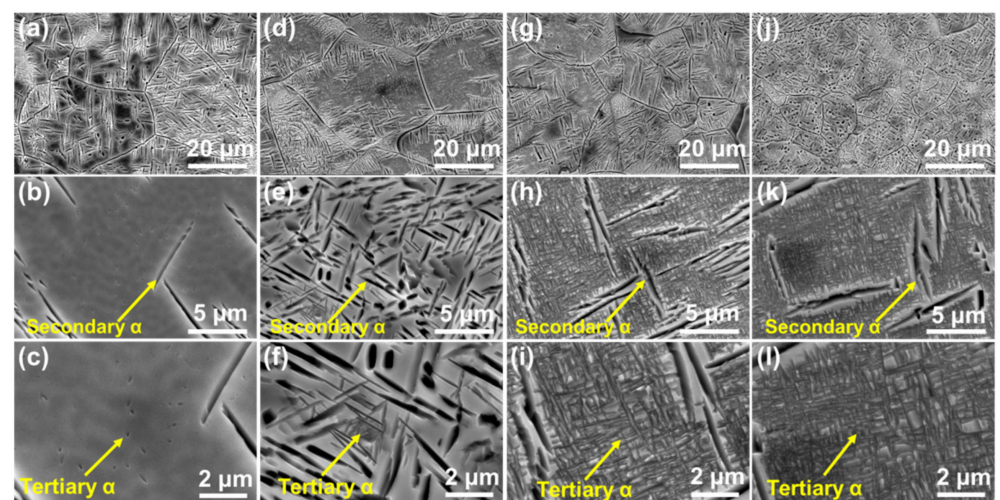


Figure 6. Microstructures of the alloy after HLDA for different time at 550 °C: (a–c) 5 min, (d–f) 0.5 h, (g–i) 2 h, (j–l) 4 h.

From the above research results, the following conclusions can be drawn:

- (1) During the HLDA process, with the prolonging of the second-step aging time, the morphology of α_T in PFZs changes from dot-like to needle-like, and its number and volume fraction increase gradually. In addition, increasing the second-step aging temperature can promote the precipitation of α_T , and the size of α_T is slightly increased.
- (2) The amount and size of α_S obtained by single aging do not change significantly after duplex aging, which indicated that it had certain stability.

As shown in Figure 7, TEM samples were subjected to 780 °C/0.5 h + 650 °C/4 h + 500 °C/4 h treatment. TEM results show that a needle-like mixture morphology for α phase which is composed of α_S (micron size in width) and α_T (nanoscale size in width) is formed after duplex aging (Figure 7b). Singh et al. [23] showed that nucleation bursts at larger undercooling (or lower temperatures) were responsible for the third generation of precipitates. In addition, because these subsequent precipitations were formed at larger undercoolings, they are typically finer in size scale. Ivasishin et al. [24] showed that at high-temperature aging, the phase transformation driving force of the alloy is small, but the solute diffusion rate is fast, so it is easy to form large size α phase. At low-temperature aging, the driving force of phase transformation is stronger, but the solute diffusion rate is slower, so a large number of small-size α phases are formed.

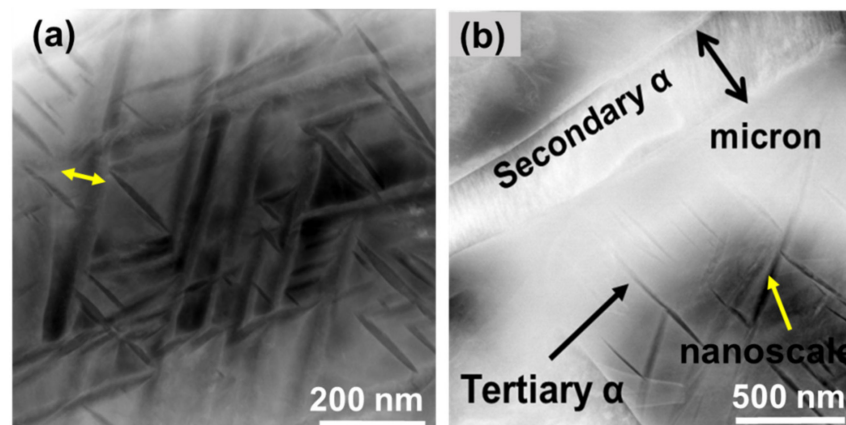


Figure 7. TEM (transmission electron microscopy) microstructures after heat treatment at 780 °C/0.5 h + 650 °C/4 h + 500 °C/4 h: (a) microstructure of α phase, (b) formation of multi-scale structure.

Figure 8 shows the sketch map of duplex aging strengthening β titanium alloy. What happens in the SA is incomplete aging. The α_S of micron size is precipitated and forms PFZs after SA at 650 °C. At this time, the temperature is higher, and the driving force for nucleation of the α phase inside the grain is small, but the driving force for growth is large, so the number of α phase precipitation at this stage is small, but the size is larger. Secondly, during HLDA from 450 °C to 550 °C, the β phase in the PFZs changes to α phase, which can obtain α_T of a size from nanocrystalline to ultrafine. At this time, the temperature is low, even if the driving force for the nucleation of the α phase is large, but the driving force for growth is small. Therefore, the number of α phase precipitated at this stage is large, but the size is small.

3.2. Mechanical Properties

In general, β -grains have good plasticity but moderate strength after solution treatment. During the subsequent aging treatment, the more α phase, the more uniform the precipitation and the higher the alloy strength. Therefore, the relationship between microstructure and mechanical properties of the alloy after different heat treatments was investigated by tensile tests at room temperature.

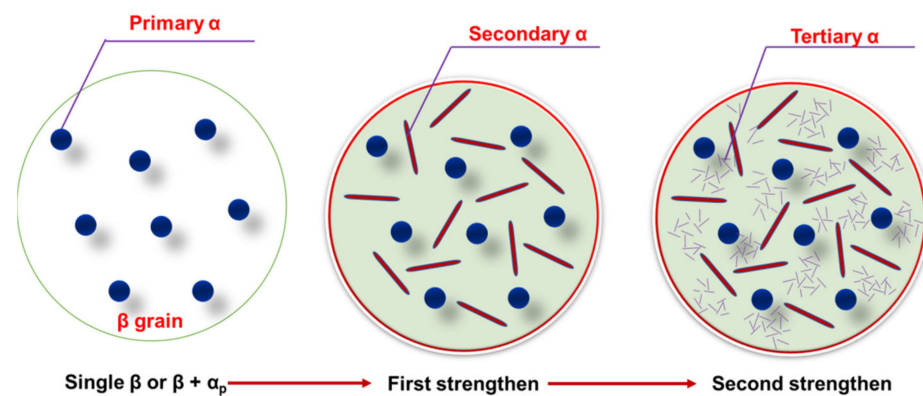


Figure 8. Sketch map of duplex-aging-strengthened β titanium alloy.

Figure 9 presents the tensile properties after different heat treatments. As shown in Figure 9a, R_m , R_p , and A represent yield strength, tensile strength, and elongation, respectively. The tensile strength is the maximum stress value before fracture. Yield strength is a stress value that produces 0.2% residual deformation. Elongation is calculated by the length before and after stretching ($A = \frac{L_1 - L_0}{L_0} \times 100\%$). The plasticity for evaluating metal materials includes elongation (elongation) A and area shrinkage Z . In this paper, plasticity (ductility) is evaluated by using elongation A , and strength is evaluated by using tensile strength.

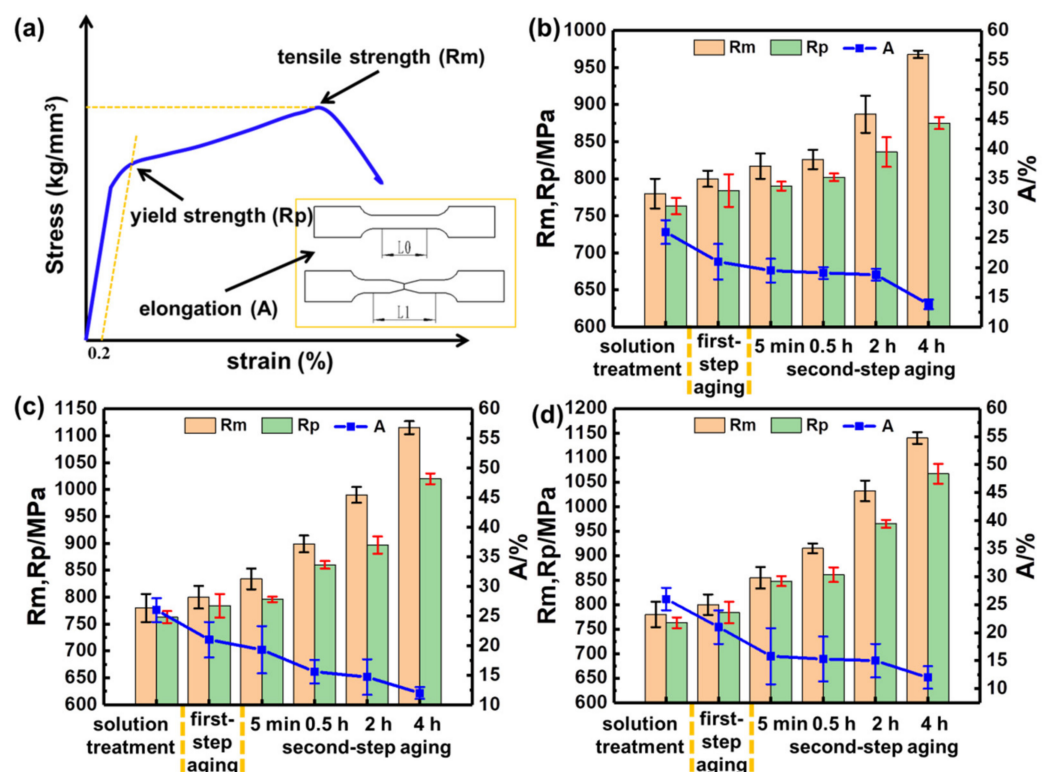


Figure 9. Mechanical properties after different HLDA: (a) diagram of the stretch symbol, (b) 450 °C, (c) 500 °C, (d) 550 °C.

After HT, the tensile strength and yield strength of the alloy are 780 MPa and 763 MPa, and the elongation is 26%. Below the phase transition point, the microstructure was composed of a very small amount of α_p and β -grain (Figure 2a). The plasticity of β -phase is better than that of solution tissue in α/β phase region, so the alloy exhibits good plasticity macroscopically. Compared with HT, the SA alloy shows a yield strength of 784 MPa with

an elongation of 21%. Generally speaking, the α_S that precipitates during aging has a very obvious strengthening effect, but it can be seen that the plasticity of SA alloy is slightly decreased. This is because the number of α_S is small, and so the strengthening effect is weak. For HLDA alloy, when at the same second aging temperature, the strength increases and the plasticity decreases with prolonging aging time. It is well known that the properties of alloys are directly proportional to the number of secondary α phases and inversely proportional to size [25,26]. Therefore, it can be seen from Figure 4d that the volume fraction of α phase in the alloy increases with the increase of HLDA time, and the α_T is fine, uniform, and dispersed. In addition, the increase of second-step aging temperature can promote the growth of α_T , and increase the volume fraction of fine α precipitates, which can significantly improve the properties of the materials. For example, when HLDA was for 4 h at 550 °C, the strength reached the maximum, the tensile strength and yield strength reached 1140 MPa and 1067 MPa, and the elongation remained at 12% (Figure 9d).

3.3. Effect of Multiscale α on Tensile Deformation Behavior

During the preparation of multiscale α phase, the alloy underwent a transition from incomplete aging to complete aging. In situ tensile testing of HT, SA, and HLDA alloys was carried out in order to further understand the relationship between microstructure and tensile deformation behavior.

Figure 10 shows the in situ tensile SEM images of HT alloy, which is composed of β matrix and a small amount of α_P (Figure 10a). In the initial stage of tensile testing, a large number of intersecting and parallel slip lines appear in the β -grains (Figure 10b). With the increase of strain, the β grains are elongated and deformed along the tensile direction (Figure 10c), and the cracks initiate along the slip system with large deformation (Figure 10e) and mainly exhibit transgranular fractures (Figure 10). In addition, the α_P is too small to be significant. Slip is the plastic deformation of a metal, and the slip band plays a role of deformation coordination and homogenization, which indicates that the material has undergone a large plastic deformation before fracture, so HT alloy exhibits excellent plasticity.

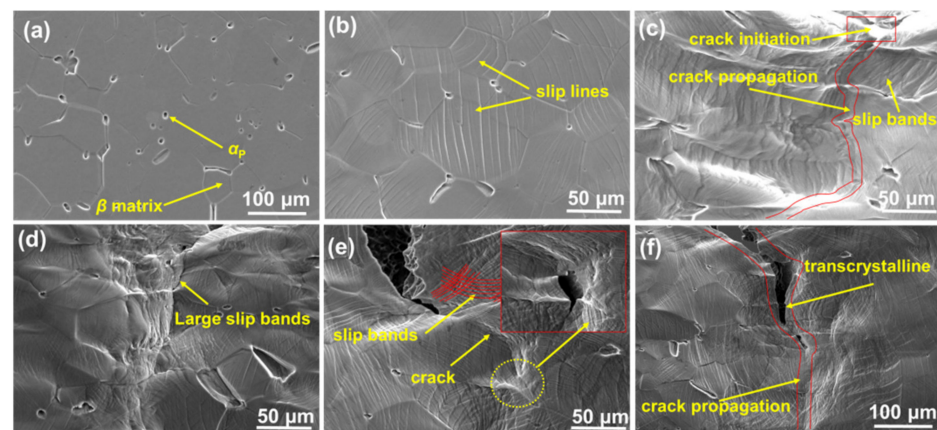


Figure 10. In situ tensile testing process of HT alloy: (a) $\varepsilon = 0$, (b) $\varepsilon = 0.10$, (c) $\varepsilon = 0.26$, (d) $\varepsilon = 0.34$, (e) $\varepsilon = 0.53$, (f) $\varepsilon = 0.67$.

Figure 11 shows the in situ tensile SEM images of SA alloy, which is obviously composed of α_S and the PFZs on the β matrix. In the initial stage of strain, the grain boundary is torn, and multiple slip lines are still observed in the PFZs (Figure 11a). With the increase of strain, the crack originates from the precipitation region at the notch. At this time, the α_S has appeared in some grains, but the α_S hardly exists in other grains. The crack passes through these grains to form a transgranular crack. As shown in Figure 11b, red areas (1) transform into red areas (2). It shows that the crack propagates in grains without precipitation, and the region without α phase can hardly hinder the deformation of the β matrix, so the propagation mode is similar to the HT process, that is, where the β grains are

elongated and deformed until the deformation exceeds the limit of the alloy, and eventually a transgranular crack is formed in this region (Figure 11c). When the crack propagates in grains with α_S group, the crack will pass through the α_S to form a transgranular fracture (red areas (3) of Figure 11b), and some grains will also form secondary cracks (Figure 11d).

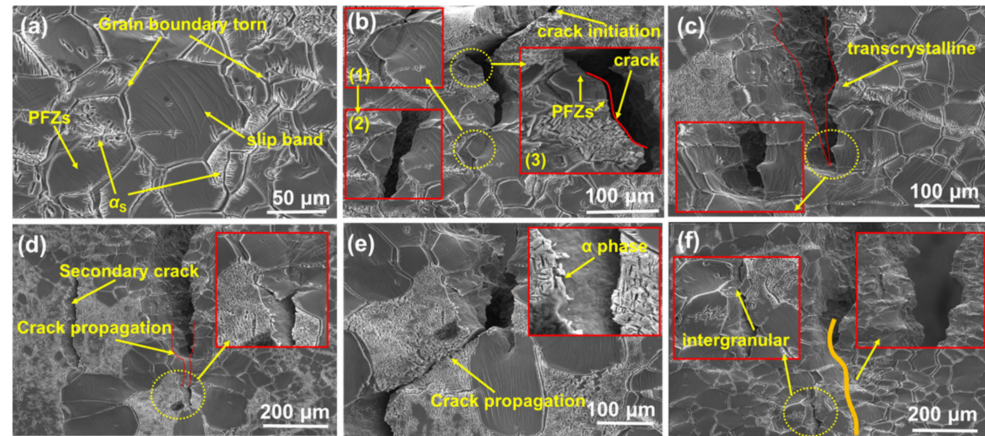


Figure 11. In situ tensile testing process of SA alloy (a) $\varepsilon = 0.10$, (b) $\varepsilon = 0.26$, (c) $\varepsilon = 0.34$, (d) $\varepsilon = 0.41$, (e) $\varepsilon = 0.53$, (f) $\varepsilon = 0.67$.

Shao [27] observed the distribution of dislocations among the α_S in the stretching process by TEM, and the results showed that the dislocations would be concentrated in the coarse α_S , and the higher local dislocation density would cause the stress concentration, which led to the formation of micropores. With the continuous increase of stress, the micropores gradually increase, and finally connect with each other or develop into microcracks. Therefore, when expanding in grains with α_S groups, the micropores are nucleated in the α phase, and gradually grow through the α_S to form a microcrack as the stress continues to increase.

In the middle stage of strain, due to stress concentration [28], a plastic deformation zone with slip line characteristics appears at the front end of the crack tip, which impedes the growth of the microcrack, and the crack will continue to expand along the α phase community (Figure 11e). A small number of grains can also easily form intergranular cracks at grain boundaries (Figure 11f), but the relatively stronger boundaries hinder their further propagation [29]. Finally, the crack propagates in a mixed mode of transgranular fracture and intergranular fracture. The results of Wu [30] show that the crack propagation is controlled by the α_S , and the coarsening of the α_S is more likely to occur with a higher aging temperature. The alloy containing the coarse α_S usually has a coarser crack front profile, which leads to higher crack propagation resistance, and ultimately, improved plasticity and fracture toughness.

In this paper, it is during first-step aging that the coarse α_S precipitates, which can increase the resistance of crack growth, so SA alloy has good ductility compared to the fine α phase of HLDA alloy. When the quantity and size of coarse α phase are controlled reasonably, the alloy can maintain good plasticity. Therefore, in the second-step aging, the fine α phase precipitated by low-temperature aging can adjust the strength, and finally achieve a good match between strength and plasticity.

Figure 12 shows the in situ tensile SEM images of HLDA alloy. After the second-step aging at 500 °C for 4 h, a large number of fine needle-like α_T are precipitated in PFZs of the previously incomplete aging. The whole matrix is filled with α phases of various sizes, and no slip lines appear in the grains (Figure 12a). Moreover, no obvious deformation occurs in the grains, indicating that the stability of the β matrix is improved. In the initial stage of strain, the β matrix is strengthened after the α_T precipitation, and the crack nucleates and grows in the region where the α_T precipitation is dense, as seen by looking at red areas (1) through red areas (3) of Figures 12b and 12c. In the relatively small α phase, the dislocations

are mainly concentrated at the α/β interface. Due to the excessive local stress between α phase and β phase, more micropores can easily form at the interface, and eventually the micropores will connect with each other and develop into intracrystalline cracks [27].

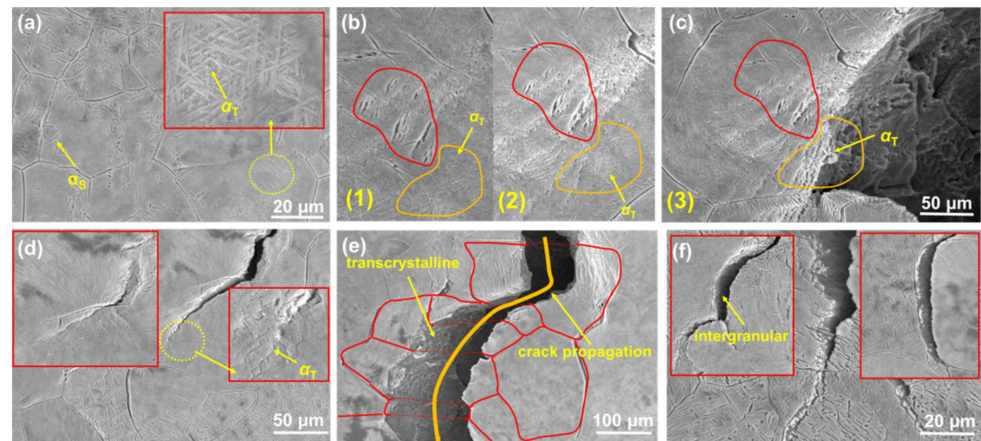


Figure 12. In situ tensile testing process of HLDA alloy (a) $\varepsilon = 0.10$, (b) $\varepsilon = 0.26$, (c) $\varepsilon = 0.34$, (d) $\varepsilon = 0.41$, (e) $\varepsilon = 0.53$, (f) $\varepsilon = 0.67$.

After second-step aging, it can be found that the size of α_T is relatively small, which will lead to crack propagation along the tertiary α/β interface within the grain to form transgranular fracture, which is the most important fracture mode (Figure 12d,e). Guo et al. [31] found that the dislocations could easily pass through the extremely fine cluster α phase and continue to move, so that both the deformation and the dislocations were concentrated in the β -grain, leading to the formation of transgranular cracks in the β -grain. A small number of grains can also easily form intergranular cracks propagating along the grain boundaries (Figure 12f). After second-step aging, a large number of small and dispersed α_T increases the strength level of the alloy, mainly because the dense needle-like α_T reduces the effective slip distance of the dislocations [32], resulting in a severe stress concentration, so the fracture behavior is almost a transgranular fracture by passing or cutting through α phase macroscopically. It is because the coarse α_S precipitates during first step-aging and forms a multiscale structure with α_T that the alloy can maintain a certain plasticity while improving its strength.

4. Conclusions

1. The microstructure composed by multiscale α phase can be obtained by high/low-temperature two-step aging heat-treatment in a descending order. In first-step high-temperature aging, the purpose of the coarse α phase obtained is to maintain a certain plasticity of the alloy, and the reserved precipitate-free zones are aimed at precipitating nanoscale (width) tertiary α phase in the second-step low-temperature aging process and enhancing the strength of the alloy. Finally, a needle-like mixture morphology, which is composed of secondary α phase (micron size in width) and tertiary α phase (nanoscale size in width), is formed after duplex aging.
2. For the microstructure, a certain amount of lath secondary α precipitated from the matrix and from the PFZs after first-step aging. During the second-step aging process, with the prolonging of second-step aging time, the morphology of tertiary α phase in PFZs changes from dot-like to needle-like, and its number and volume fraction increase gradually. In addition, increasing the second-step aging temperature can promote the precipitation of tertiary α phase, and the size of tertiary α phase is slightly increased. After second-step aging for 4 h at 550 °C, the concentration of the tertiary α phase distribution of the alloy is the densest.
3. For mechanical properties, secondary α that precipitates during first-step aging has a very obvious strengthening effect, but it can be seen that the plasticity is slightly

decreased. At the same second-step aging temperature, with the increase of aging time, the alloy macroscopically shows the characteristics of strength increase and plasticity decrease. At the same second-step aging time, increasing the aging temperature can further increase the strength of the alloy. After second-step aging at 550 °C for 4 h, the alloy properties of tensile strength and yield strength reach 1115 MPa and 1020 MPa, respectively, and the elongation is 12%.

4. In situ tensile testing of solution treatment, first-step aging, and second-step aging of alloys were carried out in order to understand the relationship between microstructure and mechanical properties. After solution treatment, a microstructure of the alloy was composed of β matrix and a small amount of primary α phase. During the stage of tensile testing, a large number of intersecting and parallel slip lines appear in the β -grains, and the cracks initiate along the slip system with large deformation and mainly exhibit transgranular fracture. Therefore, the alloy can exhibit excellent plasticity. After first-step aging, the secondary α phase has appeared in some grains. The crack passes through these grains to form a transgranular crack, and other grains will also form secondary cracks. Finally, the crack propagates in a mixed mode of transgranular fracture and intergranular fracture. Coarse secondary α phase precipitates can increase the resistance of crack growth, so the alloy still has good ductility. After second-step aging, a large number of tertiary α phase precipitates in the PFZs region of the grain, and the crack nucleates and grows in the region where the tertiary α phase precipitation is dense. A large number of small and dispersed tertiary α phase increases the strength level of the alloy. It is because the coarse secondary α phase precipitates during first-step aging and forms a multiscale structure with tertiary α phase that the alloy can maintain a certain plasticity while improving its strength.

Author Contributions: Conceptualization, Z.D.; data curation, T.G.; formal analysis, T.G.; investigation, H.J. and D.W.; methodology, D.W., X.C., F.L., J.C. and W.C.; project administration, H.J. and Z.D.; supervision, X.C.; validation, H.J.; writing—original draft, H.J.; writing—review and editing, Z.D. All authors have read and agreed to the published version of the manuscript.

Funding: This research was funded by National Natural Science Foundation of China (Grant No. 52071185 and 51861029), Program for Young Talents of Science and Technology in Universities of Inner Mongolia Autonomous Region (Grant No. NJYT-19-B25), Inner Mongolia Natural Science Foundation (Grant No. 2020MS05034), and Natural Science Foundation of Shandong Province (Grant No. ZR2019MEM037).

Institutional Review Board Statement: Not Applicable.

Informed Consent Statement: Not Applicable.

Data Availability Statement: Data sharing is not applicable to this article.

Conflicts of Interest: The authors declare no conflict of interest.

References

1. Kolli, R.P.; Devaraj, A. A Review of Metastable Beta Titanium Alloys. *Metals* **2018**, *8*, 506. [[CrossRef](#)]
2. Yumak, N.; Aslantas, K. A review on heat treatment efficiency in metastable β titanium alloys: The role of treatment process and parameters. *J. Mater. Res. Technol.* **2020**, *6*, 15360–15380. [[CrossRef](#)]
3. Gheysarian, A.; Abbasi, M.J. Aging of the β 21S Titanium Alloy. *Mater. Eng. Perform.* **2017**, *26*, 374–382. [[CrossRef](#)]
4. Ge, P.; Zhou, W.; Zhao, Y.Q.; Zhou, L. Aging characteristics of new metastable beta titanium alloy. *Trans. Nonferrous Met. Soc. China* **2007**, *17*, S88–S92.
5. Yumak, N.; Aslantas, K. Effect of Heat Treatment Procedure on Mechanical Properties of Ti-15V-3Al-3Sn-3Cr Metastable β Titanium Alloy. *J. Mater. Eng. Perform.* **2021**, *30*, 1066–1074. [[CrossRef](#)]
6. Yumak, N.; Aslantas, K.; Cetkin, A. Cryogenic and aging treatment effects on the mechanical properties of Ti-15V-3Al-3Cr-3Sn titanium alloy. *J. Test. Eval.* **2021**, *5*, 3221–3233. [[CrossRef](#)]
7. Rohit, B.; Rao, N.M. Crack nucleation in β titanium alloys under high cycle fatigue conditions—A review. *J. Phys. Conf. Ser.* **2017**, *843*, 012048.

8. Schmidt, P.; El-Chaikh, A.; Christ, H.J. Effect of duplex aging on the initiation and propagation of fatigue cracks in the so-lute-rich metastable β titanium alloy Ti 38-644. *Metall. Mater. Trans. A-Phys. Metall. Mater. Sci.* **2011**, *9*, 2652–2667. [[CrossRef](#)]
9. Santhosh, R.; Geetha, M.; Saxena, V.K.; Nageswararao, M. Studies on single and duplex aging of metastable beta titanium alloy Ti-15V-3Cr-3Al-3Sn. *J. Alloys Compd.* **2014**, *605*, 222–229. [[CrossRef](#)]
10. Furuhashi, T.; Maki, T.; Makino, T. Microstructure control by thermomechanical processing in β -Ti-15-3 alloy. *J. Mater. Process. Technol.* **2001**, *117*, 318–323. [[CrossRef](#)]
11. Mantri, S.A.; Choudhuri, D.; Behera, A.; Cotton, J.D.; Kumar, N.; Banerjee, R. Influence of Fine-Scale Alpha Precipitation on the Mechanical Properties of the Beta Titanium Alloy Beta-21S. *Metall. Mater. Trans. A-Phys. Metall. Mater. Sci.* **2015**, *7*, 2803–2808. [[CrossRef](#)]
12. Mantri, S.A.; Choudhuri, D.; Alam, T.; Viswanathan, G.B.; Sosa, J.M.; Fraser, H.L.; Banerjee, R. Tuning the scale of α precipitates in β -titanium alloys for achieving high strength. *Scr. Mater.* **2018**, *154*, 139–144. [[CrossRef](#)]
13. Santhosh, R.; Geetha, M.; Rao, M.N. Recent Developments in Heat Treatment of Beta Titanium Alloys for Aerospace Applications. *Trans. Indian Inst. Met.* **2017**, *70*, 1681–1688. [[CrossRef](#)]
14. El Chaikh, A.; Schmidt, P.; Christ, H.J. Fatigue properties of duplex-aged Ti 38-644 metastable beta titanium alloy. *Procedia Eng.* **2010**, *2*, 1973–1982. [[CrossRef](#)]
15. Li, T.; Kent, D.; Sha, G.; Cairney, J.M.; Dargusch, M.S. The role of ω in the precipitation of α in near- β Ti alloys. *Scr. Mater.* **2016**, *117*, 92–95. [[CrossRef](#)]
16. Chou, Y.K.; Tsay, L.W.; Chen, C. Effects of Aging Treatments on the Mechanical Behavior of Ti-15V-3Cr-3Sn-3Al Alloy. *J. Mater. Eng. Perform.* **2015**, *24*, 3365–3372. [[CrossRef](#)]
17. Du, Z.X.; Liu, G.L.; Liu, F.; Cheng, J.; Chen, Y.F. Influence of pre-aging on microstructure and mechanical properties of coarse grained β titanium alloy. *Rare Metal. Mat. Eng.* **2019**, *48*, 770–774.
18. Du, Z.X.; He, Q.W.; Chen, R.R.; Liu, F.; Zhang, J.Y.; Yang, F.; Zhao, X.P.; Cui, X.M.; Cheng, J. Rolling reduction—Dependent deformation mechanisms and tensile properties in a β titanium alloy. *J. Mater. Sci. Technol.* **2022**, *104*, 183–193. [[CrossRef](#)]
19. Yao, X.; Liu, S.J.; Cui, C.X.; Cai, F.F. The study on microstructure and properties of a new metastable beta titanium alloy after aging treatment. *Adv. Mater. Res.* **2011**, *1378*, 782–786. [[CrossRef](#)]
20. Lu, K. Nanocrystalline metals crystallized from amorphous solids: Nanocrystallization, structure, and properties. *Mater. Sci. Eng. R-Rep.* **1996**, *4*, 161–221. [[CrossRef](#)]
21. He, G.; Eckert, J.; Loser, W.; Schultz, L. Novel Ti-base nanostructure–dendrite composite with enhanced plasticity. *Nat. Mater.* **2003**, *1*, 33–37. [[CrossRef](#)] [[PubMed](#)]
22. Malinov, S.; Sha, W.; Markovskiy, P. Experimental study and computer modelling of the $\beta \Rightarrow \alpha + \beta$ phase transformation in β 21s alloy at isothermal conditions. *J. Alloys Compd.* **2003**, *1*, 110–118. [[CrossRef](#)]
23. Singh, A.R.P.; Nag, S.; Chattopadhyay, S.; Ren, Y.; Tiley, J.; Viswanathan, G.B.; Fraser, H.L.; Banerjee, R. Mechanisms related to different generations of γ' precipitation during continuous cooling of a nickel base superalloy. *Acta Mater.* **2013**, *1*, 280–293. [[CrossRef](#)]
24. Ivasishin, O.M.; Markovskiy, P.E.; Semiatin, S.L.; Ward, C.H. Aging response of coarse- and fine-grained β titanium alloys. *Mater. Sci. Eng. A* **2005**, *405*, 296–305. [[CrossRef](#)]
25. Lei, Z.L.; Chen, Y.; Ma, S.C.; Zhou, H.; Liu, J.T.; Wang, X.F. Influence of aging heat treatment on microstructure and tensile properties of laser oscillating welded TB8 titanium alloy joints. *Mater. Sci. Eng. A* **2020**, *797*, 140083. [[CrossRef](#)]
26. Mora, L.; Quesne, C.; Penelle, R. Relationships among thermomechanical treatments, microstructure, and tensile properties of a near beta-titanium alloy: β -CEZ: Part II. Relationships between thermomechanical treatments and tensile properties. *J. Mater. Res.* **1996**, *11*, 89–99. [[CrossRef](#)]
27. Zhao, M.J. Growth Behavior of α -Phase in Ti-55531 Alloy and Its Effect on Tensile Fracture. Master's Thesis, Xi'an University of Technology, Xi'an, China, 2019.
28. Shao, H.; Zhao, Y.Q.; Ge, P.; Zeng, W.D. In-situ SEM observations of tensile deformation of the lamellar microstructure in TC21 titanium alloy. *Mater. Sci. Eng. A* **2013**, *559*, 515–519. [[CrossRef](#)]
29. Zhao, Q.Y.; Yang, F.; Torrens, R.; Bolzoni, L. In-situ observation of the tensile deformation and fracture behaviour of powder-consolidated and as-cast metastable beta titanium alloys. *Mater. Sci. Eng. A* **2019**, *750*, 45–59. [[CrossRef](#)]
30. Wu, C.; Zhan, M. Effect of solution plus aging heat treatment on microstructural evolution and mechanical properties of near- β titanium alloy. *Trans. Nonferrous Met. Soc. China* **2019**, *29*, 997–1006. [[CrossRef](#)]
31. Guo, S.; Meng, Q.K.; Liao, G.Y.; Hu, L.; Zhao, X.Q. Microstructural evolution and mechanical behavior of metastable β -type Ti-25Nb-2Mo-4Sn alloy with high strength and low modulus. *Prog. Nat. Sci.* **2013**, *23*, 174–182. [[CrossRef](#)]
32. Liu, A.J.; Wang, L.; Dai, H.X. Effect of Heat Treatment on the Microstructure and Dynamic Behavior of Ti-10V-2Fe-3Al Alloy. In Proceedings of the Symposium on Explosion, Shock Wave and High-Strain-Rate Phenomena, Beijing, China, 25–26 September 2016; pp. 155–160.